Boundary-Layer Meteorology (2019) 170:489–505
https://doi.org/10.1007/s10546-018-0407-x

RESEARCH ARTICLE

Surface Energy Budget Observed for Winter Wheat in the North China Plain During a Fog–Haze Event

Changwei Liu[1] · Zhiqiu Gao[2,3] · Yubin Li[3] · Chloe Y. Gao[4] · Zhongbo Su[5] · Xiaoye Zhang[6]

Received: 31 March 2018 / Accepted: 30 October 2018 / Published online: 27 November 2018

Abstract
In recent winters, fog–haze events have occurred frequently over the North China Plain. To understand the characteristics of conventional meteorological conditions, the near-surface radiation balance, and the surface energy budget under different pollution levels, we analyzed data collected at an observation site in Gucheng, which is located in the Hebei province in North China, based on a campaign that ran from December 1 2016 to January 31 2017. We found that meteorological conditions with a lower wind speed, weakly unstable (stable) stratification, higher relative humidity, and lower surface pressure during the daytime (night-time) are associated with fog–haze events. On heavy pollution days (defined as days with a daily mean $PM_{2.5}$ concentration >150 μg m^{-3}), the decrease in downward shortwave radiation ($S_{\downarrow}$) and the increase in downward longwave radiation ($L_{\downarrow}$) are significant. The mean $S_{\downarrow}$ ($L_{\downarrow}$) values on clean-air days (daily mean $PM_{2.5}$ concentration <75 μg m^{-3}) and heavily polluted days was 222 (222) W m^{-2} and 124 (265) W m^{-2}, respectively. Due to the negative (positive) radiative forcing of aerosols during the daytime (night-time), the daily maximum (night-time mean) net radiation (R_n) is negatively (positively) related to the daily mean $PM_{2.5}$ concentration, the correlation coefficient between the daily maximum (night-time mean) R_n and daily mean $PM_{2.5}$ concentration being -0.47 (0.51). Diurnal variations in sensible heat flux (H) and latent heat flux (λE) are insignificant on heavily polluted days, the mean daily maximum H (λE) is only 40 (28) W m^{-2} on heavily polluted days, but reaches 90 (42) W m^{-2} on clean-air days. Additionally, the friction velocity, standard deviation of vertical velocity, and turbulent kinetic energy on heavily polluted days are also quantified.

Keywords Fog–haze event · Meteorological conditions · Near-surface radiation balance · Surface energy budget · Turbulent characteristics

1 Introduction

As the economic, industrial and cultural centre of the country, the North China Plain (NCP) is one of the most developed areas in China. However, along with rapid economic development during recent years frequently occurring fog–haze pollution events (Chan and Yao 2008; Ding and Liu 2014) are common. The associated generation mechanisms and the weather/climate

Extended author information available on the last page of the article

impacts of these heavy fog–haze events over this area have attracted increasing attention (e.g., Lin et al. 2009; Quan et al. 2011; Xu et al. 2011; Fu et al. 2014; Chen and Wang 2015). Studies have shown that the occurrence of fog–haze events is strongly related to local meteorological conditions and especially boundary-layer processes (e.g., Ramanathan et al. 2001; Zhang et al. 2014; Wang et al. 2016). By investigating the synoptic flow conditions and boundary-layer processes during severe fog–haze episodes, Ye et al. (2015) pointed out that low wind speed, high humidity, and stable stratification were related to fog–haze events in the NCP. Moreover, the surface energy budget is affected by fog–haze events through aerosol radiative forcing (Li et al. 2007; Wang et al. 2009), which can further modify atmospheric stratification and turbulent characteristics (Pahlow et al. 2005; Dupont et al. 2016). Wang et al. (2014) measured the radiative fluxes at heights of 2 m and 280 m during a typical pollution episode from October 16 to December 20, 2004 in Beijing (the largest city in the NCP region) and found that the downward shortwave radiation ($S_{\downarrow}$) at noon at 280-m height was 208 W m^{-2} on a heavily polluted day and 554 W m^{-2} on a clean air day. The divergence of $S_{\downarrow}$ between 280- and 2-m heights increased with a reduction in the PM_{10} concentration. Che et al. (2014) analyzed aerosol radiative forcing on a daily scale during a serious fog–haze month over the NCP and found that the pollutant particles imposed a cooling effect on the atmosphere through negative radiative forcing (which varied between -43 W m^{-2} and -144 W m^{-2} for different sites), and the cooling effect generally increased with the pollutant concentration. Through numerical simulations of flow over the NCP region, Gao et al. (2015) confirmed the negative radiative forcing of -20 to -140 W m^{-2} at the surface but also indicated a large positive aerosol radiative forcing of 20 to 120 W m^{-2} in the atmosphere, which further reduced the daily mean sensible heat flux (H) and latent heat flux (λE) by 5–16 W m^{-2} and 1–5 W m^{-2}, respectively.

Although the radiative forcing of aerosols has been intensively investigated, the surface energy budget under heavy pollution conditions is not thoroughly understood. To further evaluate the surface energy budget during fog–haze conditions in the NCP region, we investigate the radiation components and turbulent parameters at an hourly scale over a winter wheat field in the NCP.

2 Materials

2.1 Observation Site and Instruments

The data were collected at Gucheng (39°08′N, 115°40′E) during a campaign that ran from December 1 2016 to January 31 2017, Gucheng is located in a rural district of Hebei province, which is approximately 110 km south-east of Beijing (Fig. 1), and comprises an integrated ecological and meteorological observation station operated by the Chinese Academy of Meteorological Sciences. During the observation period, the main crop type was winter wheat, and the surface was generally flat. A meteorological tower was installed in the wheat field, and the instruments on the tower included a barometric pressure sensor CS100 by Apogee Instruments, a net radiometer CNR1 by Kipp and Zonen, a temperature and humidity sensor HMP45C by Campbell Scientific Incorporation, a three-dimensional ultrasonic anemometer CSAT-3 by Campbell Scientific Incorporation, and an open path CO_2/H_2O infrared gas analyzer LI-7500 by LI-COR Incorporation. Moreover, a soil-heat-flux plate HFT3, two soil moisture reflectometers CS615, and two averaging soil thermocouple probes TCAV by Campbell Scientific Incorporation were installed below the surface. Detailed descriptions

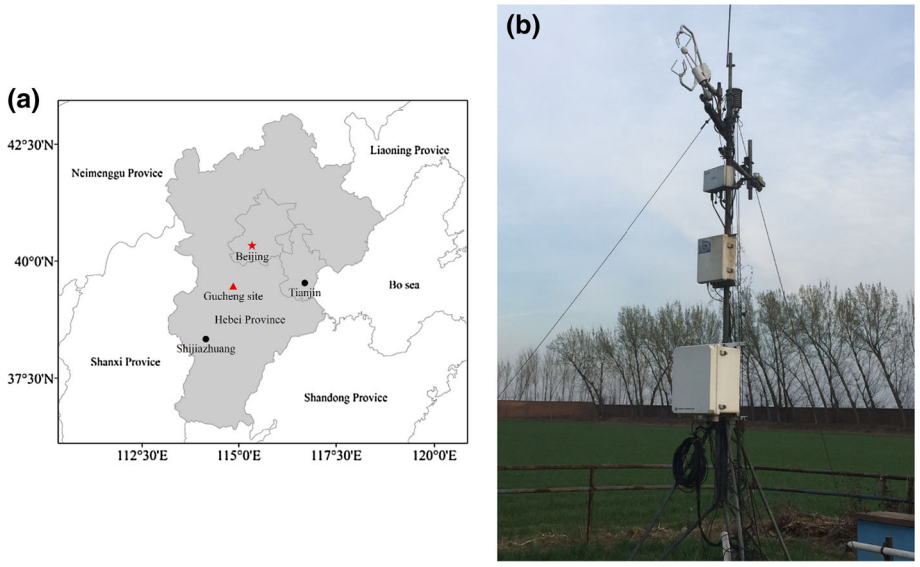

Fig. 1 **a** The geographical location of the Gucheng measurement site (marked as a red triangle), and **b** the eddy-covariance observation tower at the Gucheng measurement site

of the accuracy of these instruments and their installation heights can be found in Table 1. Additionally, an environmental dust monitor instrument with 31 different size channels at a flow rate of 1.2 L min^{-1} (EDM180 by GRIMM) was fixed at the top of an 8-m high building to collect PM2.5 concentration data. All of the data were averaged every hour, and the quality control for the data were carried out as follows:

(1) The spikes in the data series for all variables were removed by using a criterion of $X(t) < (\overline{X} - 4\sigma)$ or $X(t) > (\overline{X} + 4\sigma)$, where $X(t)$ denotes the measurements, $\overline{X}$ is the mean over the interval, and σ is the standard deviation.
(2) Sensible and latent heat fluxes were calculated using the eddy-covariance method with a 30-min averaging period. Linear detrending was first applied to the 10-Hz observations with a 30-min interval (Moncrieff et al. 2004), and the covariance was then adjusted by double rotation. Lastly, a virtual temperature correction for H and a density correction for λE were employed (Webb et al. 1980). In addition, data collected on rainy days were eliminated.
(3) Based on the method of quality control for eddy-covariance measurements proposed by Foken et al. (2012), which includes a non-stationarity test, an integrated turbulence characteristics test, and a horizontal wind-angle test, the data of class 9 were excluded.

According to the environmental air quality criteria issued by the Ministry of Environmental Protection of China, pollution conditions during the observation period were categorized into three levels: (1) clean air days, (2) moderate pollution days, and (3) heavy pollution days, when the daily mean $PM_{2.5}$ concentration is 0–75 $\mu g\ m^{-3}$, 75–150 $\mu g\ m^{-3}$, and above 150 $\mu g\ m^{-3}$, respectively.

Table 1 Type key technical specifications of sensors

Sensor type	Measurement range	Precision	Sampling frequency (Hz)	Installation height (m)
CS100	Pa: 600–1100 hPa	<0.5 hPa	0.1	4
CNR1	$S_{\downarrow}$, $S_{\uparrow}$: 0.3–3.0 μm $L_{\downarrow}$, $L_{\uparrow}$: 5–50 μm	10–35 μv W^{-1} m^{-2} 5–35 μv W^{-1} m^{-2}	0.1	3.6
HMP54C	T_a: −40–60 °C RH: 0–100%	<0.5 °C 1–90%,<2% 90–100%,<3%	0.1	4.2
CSAT3	u', v': −65–65 m s^{-1} w': −65–65 m s^{-1} T_v': −50–+60 °C	u', v': ±0.04 m s^{-1} w': ±0.02 m s^{-1} T_v': ±0.025 °C	10	4
LI-7500	q': 0–42 g m^{-3} CO_2: 0–5148 mg m^{-3}	q': ±0.02 g m^{-3} CO_2: ±0.2 mg m^{-3}	10	4
HFT3	$G_{0.05}$: −1000–+1000 W m^{-2}	±5%	0.1	0.05 m below the ground
CS615	η: 0–100%	<3%	0.1	0.05 m and 0.2 m below the ground
TCAV	T: −35–+50 °C	±0.3 °C	0.1	0.05 m and 0.2 m below the ground

2.2 Methods

Sensible and latent heat fluxes can be calculated using the eddy-covariance method for high-frequency observations, as

$$H = \rho c_p \overline{w'\theta'}, \tag{1}$$

$$\lambda E = \lambda \rho \overline{w'q'}, \tag{2}$$

where w', θ', and q' are the turbulent fluctuations of the vertical velocity, the potential temperature, and the water vapour density, respectively, ρ is the air density, c_p is the specific heat capacity of air at constant pressure, and λ is the latent heat of vapourization. The surface energy balance can be written as (the residual energy is ignored)

$$R_n = S_\downarrow - S_\uparrow + L_\downarrow - L_\uparrow, \tag{3}$$

$$R_n = H + \lambda E + G_0, \tag{4}$$

where R_n is the net radiation, $S_\downarrow$, $S_\uparrow$, $L_\downarrow$, and $L_\uparrow$ are the downward shortwave radiation, the upward shortwave radiation, the downward longwave radiation, and the upward longwave radiation fluxes, respectively. In addition, G_0 is the surface soil heat flux that can be calculated from

$$G_0 = G_{0.05} + C_g \Delta z(\partial T/\partial t), \tag{5}$$

$$C_g = (1 - \eta_s)C_s + \eta C_w, \tag{6}$$

where $G_{0.05}$ is the soil heat flux at 0.05-m depth, C_g is the volumetric heat capacity of the soil, Δz is the thickness of a thin layer of the soil, T is the mean soil temperature of the thin layer, η is the volumetric moisture content, η_s is the saturation value of η, and C_s is the volumetric heat capacity of soil. For different soil types, Garratt (1992) gave the corresponding values of η_s and C_s. At the Gucheng measurement site, the soil type is clay, which results in η_s and C_s values of 0.482 J m^{-3} K^{-1} and 2.106×10^6 J m^{-3} K^{-1}, respectively, C_w is the water volumetric heat capacity, taken as 4.186×10^6 J m^{-3} K^{-1}.

The surface temperature (T_s) can be calculated from the Stefan–Boltzmann relation,

$$T_s = ((L_\uparrow - (1 - \varepsilon)L_\downarrow)/(\varepsilon_s \sigma_s))^{1/4}, \tag{7}$$

where σ_s is the Stefan–Boltzmann constant and ε_s is the surface emissivity, set as 0.96 according to the type of surface cover (Garratt 1992).

To analyze the characteristics of turbulence, the following turbulent parameters are used,

$$u_* = (\overline{u'w'})^{1/2}, \tag{8}$$

$$\sigma_w = (\overline{w'^2})^{1/2}, \tag{9}$$

$$e = \frac{1}{2}(\overline{u'^2} + \overline{v'^2} + \overline{w'^2}), \tag{10}$$

where u_*, σ_w, and e are the friction velocity, the standard deviation of vertical velocity, and the turbulent kinetic energy (TKE), respectively, u' and v' are the turbulent fluctuations of the horizontal velocity along the x and y axis, respectively.

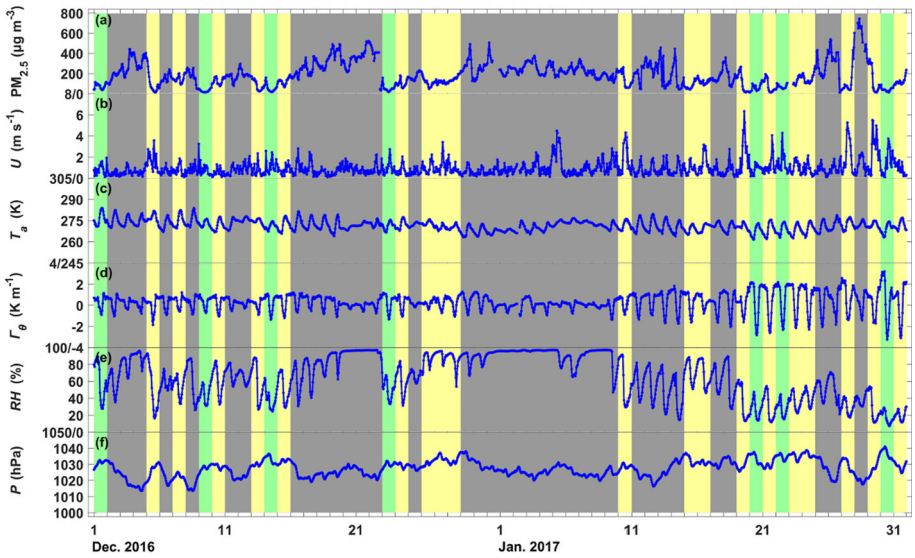

Fig. 2 Meteorological data collected during the period from December 1 2016 to January 31 2017 at the Gucheng measurement site. **a**–**f** Are the time series of $PM_{2.5}$ concentration, wind speed, air temperature, vertical potential temperature gradient, relative humidity, and pressure (p), respectively. The green blocks, yellow blocks, and grey blocks represent clean-air days, moderately polluted days, and highly polluted days, respectively

3 Results

3.1 Conventional Meteorological Conditions

Figure 2 shows the time series of the observed $PM_{2.5}$ concentration, wind speed, air temperature, vertical potential temperature gradient ($\Gamma_\theta = (T_a - T_s)/z$, where T_a is the air temperature and z is the observation height), relative humidity, and air pressure. It can be seen that there were seven clean-air days, 19 moderately polluted days and 36 highly polluted days from December 1 2016 to January 31 2017. The mean $PM_{2.5}$ concentration on clean-air days, moderately polluted days, and highly polluted days was 54, 118, and 252 $\mu g\ m^{-3}$, respectively. During the observation period, light rain occurred on December 26 2016 (2 mm) and January 7 2017 (1.4 mm). Shown in Fig. 2a, precipitation reduced the $PM_{2.5}$ concentration via wet deposition. The wind speed at 4-m height was relatively low throughout the observation period, and the mean wind speed on clean-air days, moderately polluted days, and highly polluted days was 1.5, 1, and 0.8 m s^{-1}, respectively (Fig. 2b). The correlation coefficient between daily mean $PM_{2.5}$ concentration and daily mean wind speed was -0.23, with the correlation coefficient between daily mean $PM_{2.5}$ concentration and daily maximum wind speed equal to -0.35. The negative correlation coefficients indicated that a higher $PM_{2.5}$ concentration was generally accompanied by lower wind speed, and the larger correlation coefficient for daily maximum wind speed indicated that it related more closely with daily mean $PM_{2.5}$ concentration than with daily mean wind speed. For the air temperature at 4.2-m height (Fig. 2c), the whole-averaged value was 271.4 K. The variation of air temperature did not present a significant correlation to the variation of $PM_{2.5}$ concentration, though it was closely related to the synoptic process. As shown in Fig. 2d, the atmosphere was stable in

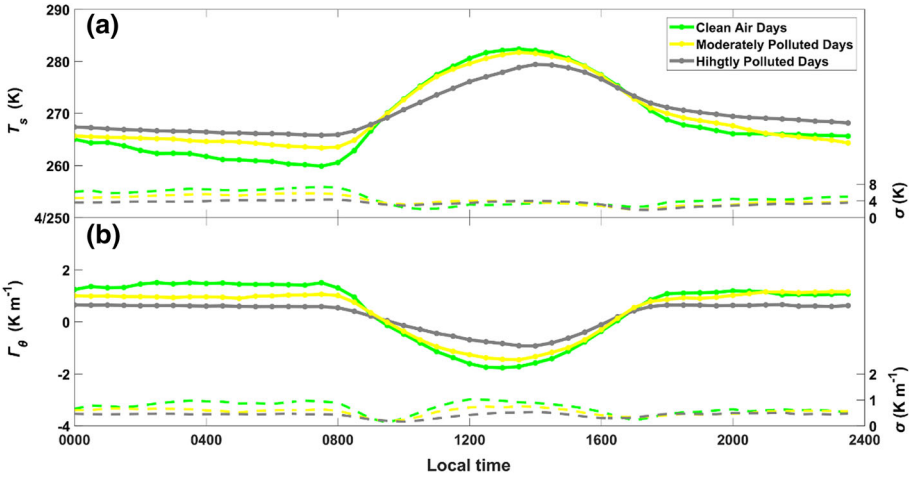

Fig. 3 The mean diurnal variation of **a** surface temperature and **b** Γ_θ under different conditions of pollution. The green line, yellow line, and grey line represent the mean value on clean air days, moderately polluted days, and highly polluted days, respectively, dash lines are standard deviation (σ)

the evening, but in the daytime, the atmosphere was unstable during the whole observation period. The mean vertical potential temperature gradient in night-time (daytime) was 0.8 (-0.4) K m^{-1}. At the 4.2-m height, the mean relative humidity on clean air days, moderately polluted days, and highly polluted days was 38%, 52%, and 75%, respectively, and the correlation coefficient between the daily mean $PM_{2.5}$ concentration and daily mean relative humidity was 0.47. Seen from Fig. 2f, highly polluted days generally corresponded to lower pressure at 4-m height, which is unfavourable for the dispersion of pollutants (Zhao et al. 2013). The mean pressure on clean-air days, moderately polluted days, and highly polluted days was 1032 hPa, 1030 hPa, and 1025 hPa, respectively, and the correlation coefficient between the daily mean $PM_{2.5}$ concentration and daily mean pressure was -0.56.

Figure 3 presents the mean diurnal variation of surface temperature and Γ_θ on clean-air days, moderately polluted days, and highly polluted days. Figure 3a shows that during the daytime, the surface temperatures on clean-air days and moderately polluted days are almost equal, but the surface temperature on highly polluted days was lower than that on clean-air days or moderately polluted days. The mean daily maximum surface temperature on highly polluted days was 279.4 K, but on clean-air days (moderately polluted days), it was 282.3 (281.7) K. After sunset, the surface temperature decreased more rapidly on clean-air days than on highly polluted days, and the surface temperature at night-time on highly polluted days was higher than that on clean-air days, showing a warming effect of aerosols. From Fig. 3b, it is noteworthy that the unstable stratification during the daytime (or stable stratification at night-time) for highly polluted days was weaker than that on clean-air days or moderately polluted days, presumably due to the surface cooling (warming) effect of aerosols during the daytime (night-time).

3.2 Radiation Components

Through absorption, scattering, and emission, radiation components are affected by pollutant particles. Figure 4 shows the time series of observed $S_\downarrow$, $S_\uparrow$, $L_\downarrow$, and $L_\uparrow$, noting that data

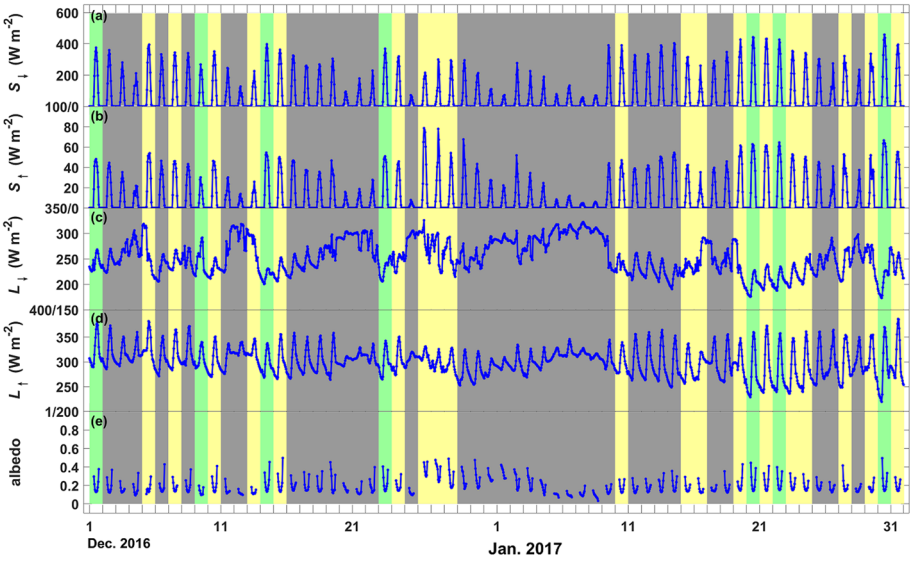

Fig. 4 Surface radiation components and albedo from December 1 2016 through January 31 2017 at the Gucheng measurement site. **a**–**e** Are $S_\downarrow$, $S_\uparrow$, $L_\downarrow$, $L_\uparrow$, and albedo, respectively. The green blocks, yellow blocks, and grey blocks represent clean-air days, moderately polluted days, and highly polluted days, respectively

collected during periods of precipitation were omitted in the following analyses. Figure 4a, b also show that lower daily average values of $S_\downarrow$ and $S_\uparrow$ occur on highly polluted days; the mean $S_\downarrow$ and $S_\uparrow$ values on highly polluted days are 124 and 19 W m^{-2}, but the mean $S_\downarrow$ and $S_\uparrow$ values on clean-air days reach 222 and 38 W m^{-2}. The correlation coefficient between daily mean $PM_{2.5}$ concentration and daily mean $S_\downarrow$ ($S_\uparrow$) was -0.54 (-0.53). The surface albedo varied around 0.14, depending mostly on the solar elevation angle and surface properties. Although there was no obvious change in air temperature related to the degree of pollution, the $L_\downarrow$ values clearly appear to be larger on highly polluted days as shown in Fig. 4c. The mean $L_\downarrow$ value on clean-air days, moderately polluted days, and highly polluted days is 222, 244, and 265 W m^{-2}, respectively, with the correlation coefficient between daily mean $PM_{2.5}$ concentration and daily mean $L_\downarrow$ equal to 0.49. Shown in Fig. 4d, $L_\uparrow$ determined by surface temperature shows an evident diurnal variation, but the daily mean $L_\uparrow$ value has no obvious change with the variation in daily mean $PM_{2.5}$ concentration.

The mean diurnal variation of $S_\downarrow$, $S_\uparrow$, $L_\downarrow$, and $L_\uparrow$ is shown in Fig. 5. The mean daily maximum $S_\downarrow$ gradually decreased from clean-air days to highly polluted days, with values of 387 and 232 W m^{-2}. For $S_\uparrow$, there was a significantly lower value on highly polluted days compared to that on clean air days, due to the associated lower $S_\downarrow$. As can be seen in Fig. 5c, the mean diurnal variation of $L_\downarrow$ on clean air days is more significant than that on moderately polluted days (or highly polluted days), due to the effect of aerosols. Figure 5d shows the mean diurnal variation of $L_\uparrow$ under different pollution conditions. The mean daily maximum $L_\uparrow$ value on highly polluted days is 13 (10) W m^{-2}, less than that on clean-air days (moderately polluted days). In order to show the radiative forcing of aerosols more intuitively on highly polluted days, Fig. 6 depicts the near-surface radiation balance at noon and midnight on clean-air days and highly polluted days. Seen in Fig. 6a, the net shortwave radiative forcing and net longwave radiative forcing at noon are -142 and 52 W m^{-2}, which results in a total radiative forcing of -90 W m^{-2} and the negative total radiative forcing in the

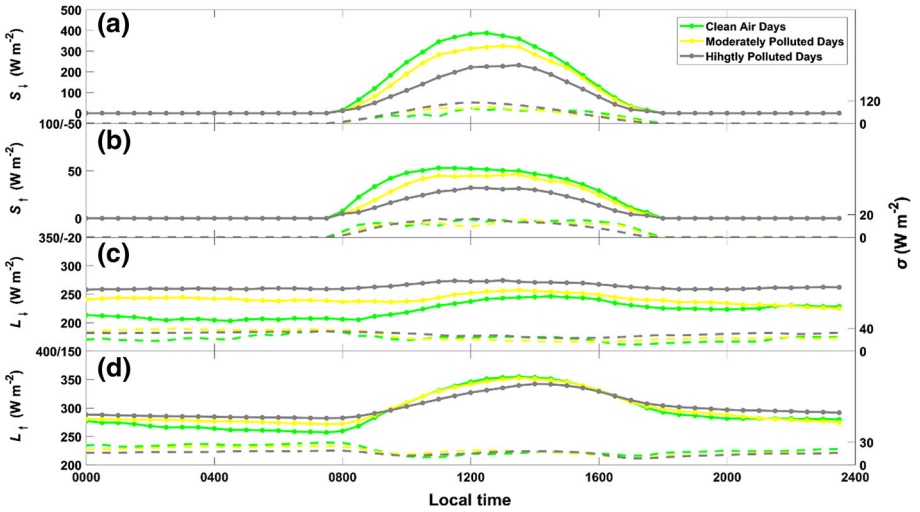

Fig. 5 The mean diurnal variation of **a** $S_{\downarrow}$, **b** $S_{\uparrow}$, **c** $L_{\downarrow}$, and **d** $L_{\uparrow}$ under different conditions of pollution. The green line, yellow line, and gray line represent the mean value on clean-air days, moderately polluted days, and highly polluted days, respectively, dash lines are σ

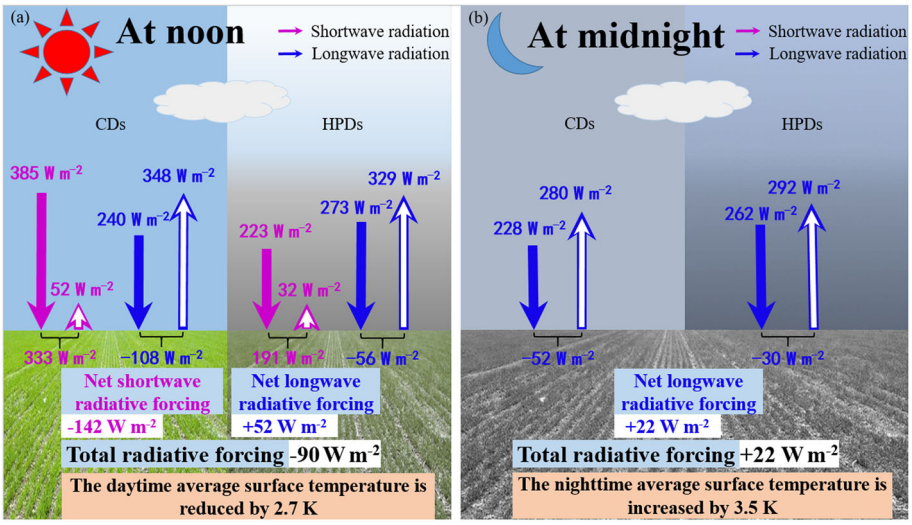

Fig. 6 A sketch map of the near-surface radiation balance. **a** The radiation balance at 1200 LT (local time = UTC + 8 h), and **b** at 2400 LT

daytime reduces the daytime average surface temperature (averaged from sunrise to sunset) by 2.7 K (refer to Fig. 3a). However, as described in Fig. 6b, the total radiative forcing is determined only by the net longwave radiative forcing, which is 22 W m^{-2} at midnight. The positive total radiative forcing at night increases the night-time average surface temperature (averaged from sunset to sunrise) by 3.5 K (refer to Fig. 3a).

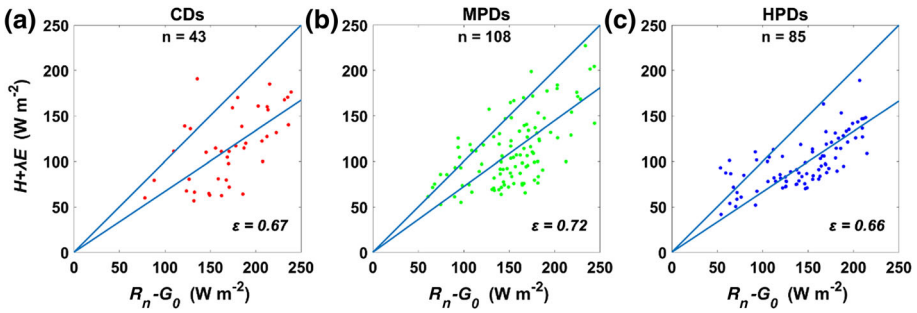

Fig. 7 Comparison between turbulent heat fluxes ($H+\lambda E$) and surface available energy (R_n-G_0) under different conditions of pollution during the period from 1 December 2016 through 31 January 2017 at the Gucheng measurement site

3.3 Surface Energy Budget

Before analyzing the surface energy budget under different pollution levels, we checked the energy balance closure (ε), defined as

$$\varepsilon = \frac{H + \lambda E}{R_n - G_0}. \tag{11}$$

Note that data with H or $\lambda E < 20$ W m^{-2} or $R_n < 100$ W m^{-2} were eliminated in the calculation of ε. Figure 7 shows that ε on clean-air days (number of sample: 43), moderately polluted days (number of sample: 108), and highly polluted days (number of sample: 85) is equal to 0.67, 0.72, and 0.66, respectively. The all-averaged value of ε is equal to 0.67, which is similar to Foken et al. (1998) for short grass. The energy imbalance may be caused by a variety of factors, such as the wave phase difference between soil surface heat flux and soil surface temperature (Gao et al. 2010), neglected vertical soil-water movement (Gao et al. 2007), as well as observation errors. In Fig. 8, during night-time, R_n is negative, H and λE are approximately zero, thus the energy loss by R_n is partly balanced by G_0. The daily maximum R_n on highly polluted days is always smaller than that on moderately polluted days or clean-air days, which is primarily caused by the smaller daily maximum $S_\downarrow$ on highly polluted days. The mean daily maximum R_n on clean-air days, moderately polluted days, and highly polluted days is 226, 183, and 135 W m^{-2}, respectively. The correlation coefficient between daily mean $PM_{2.5}$ concentration and daily maximum R_n is -0.47. However, the night-time mean R_n is positively correlated with the daily mean $PM_{2.5}$ concentration, with a correlation coefficient of 0.51. The night-time mean R_n on clean-air days, moderately polluted days, and highly polluted days is -59, -44, and -29 W m^{-2}, respectively. The cause of this phenomenon is that the night-time mean R_n is mainly determined by the longwave radiation at night while the $L_\downarrow$ is increases significantly on highly polluted days. The mean H (λE) on clean-air days, moderately polluted days, and highly polluted days is 16 (10) W m^{-2}, 13 (9) W m^{-2}, and 8 (6) W m^{-2}, respectively. The correlation coefficient between daily mean $PM_{2.5}$ concentration and daily mean H (λE) is -0.36 (-0.32).

Figure 9 illustrates the mean diurnal variation of R_n, H, λE and G_0 under different pollution conditions; as shown the daytime H and λE values decrease significantly from clean-air days to highly polluted days, with the mean daily maximum H and λE being 40 and 28 W m^{-2} on highly polluted days, while reaching 90 (81) and 42 (40) W m^{-2} on clean-air days (moderately polluted days). However, at night-time, H and λE are very small and not affected by pollution,

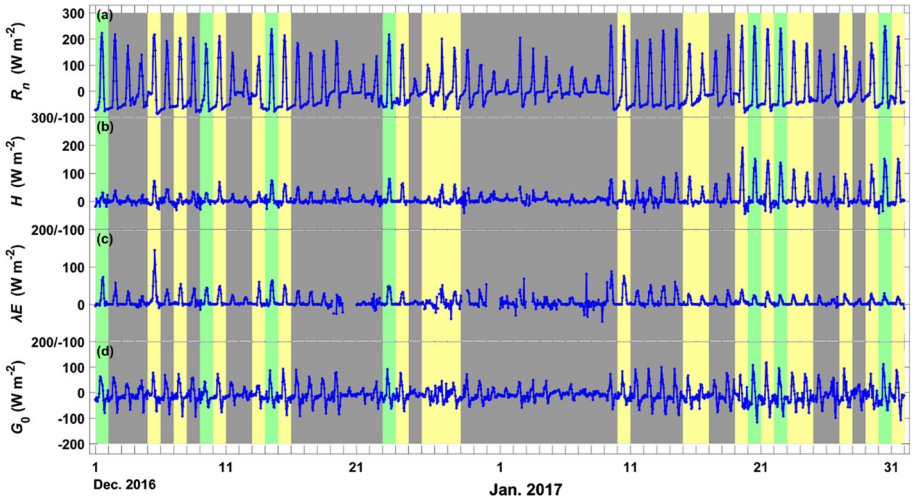

Fig. 8 Time series of **a** R_n, **b** H, **c** λE, and **d** G_0 from December 1 2016 through January 31 2017 at the Gucheng measurement site. The green blocks, yellow blocks, and grey blocks represent clean air days, moderately polluted days, and highly polluted days, respectively

and so H and λE show a smaller diurnal variation on highly polluted days than on clean-air days and moderately polluted days. For G_0, the mean daily maximum value on clean-air days, moderately polluted days, and highly polluted days is 93, 67, and 39 W m^{-2}, respectively. Figure 10 shows the difference of the surface energy budget between clean-air days and highly polluted days at noon and midnight. The reduction ratio of H, λE and G_0 caused by the aerosols is 56%, 40% and 7% at noon, respectively, as seen in Fig. 10a. The reduction ratio of G_0 is not remarkable at noon, but the G_0 daily peak, which occurs in the morning, is significantly affected by aerosols. Further, the reduction ratio of G_0 is 28% at midnight.

3.4 Turbulence Parameters

Here, the turbulent parameters including u_*, σ_w, and e are used to compare the characteristics of turbulence under different pollution levels. Figure 11 exhibits the time series of u_*, σ_w, and e with the mean u_* on clean-air days, moderately polluted days, and highly polluted days equal to 0.10, 0.11, and 0.09 m s^{-1}, respectively. There is no significant correlation between the daily mean $PM_{2.5}$ concentration and daily mean u_*, and the correlation coefficient is -0.22. However, the correlation coefficient between the daily mean $PM_{2.5}$ concentration and daily maximum u_* reaches -0.37. In Fig. 11b, the smaller values of σ_w occur on highly polluted days, with the mean σ_w on clean-air days, moderately polluted days, and highly polluted days being 0.13, 0.15, and 0.11, respectively. There is a weak negative correlation between the daily mean $PM_{2.5}$ concentration and daily mean σ_w, and the correlation coefficient is -0.26, which is indicative of a slightly reduced standard deviation of vertical velocity due to the weaker stable stratification on highly polluted days. For TKE, the mean value on clean-air days, moderately polluted days, and highly polluted days is 0.28, 0.29, and 0.18 m s^{-2}, respectively; the correlation coefficient between daily mean e and daily mean $PM_{2.5}$ concentration is -0.34.

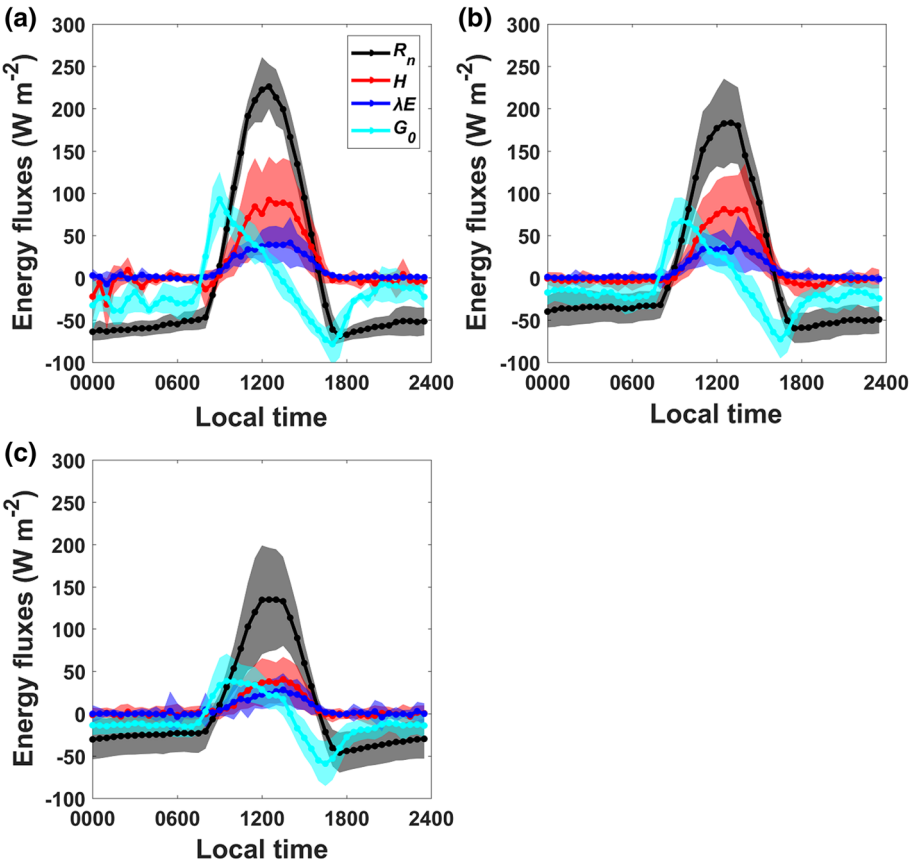

Fig. 9 The mean diurnal variation of R_n, H, λE and G_0 under **a** clean-air days, **b** moderately polluted days and **c** highly polluted days. The black line, red line, blue line, and green line represent the mean value of R_n, H, λE and G_0, respectively, shaded areas show σ

The mean diurnal variation of u_*, σ_w and e on clean-air days, moderately polluted days, and highly polluted days is shown in Fig. 12. The u_*, σ_w and e values all show a diurnal variation with low values at night and high values during the daytime. In general, the value of u_* is small throughout the observation period, although the mean daily maximum u_* on clean-air days reaches 0.23 m s^{-1}. Nevertheless, a distinctly different diurnal variation of u_* under different pollution levels is found in Beijing (Guo et al. 2016). Their results show a notably larger u_* on clean-air days than on highly polluted days. However, our results show that the difference of u_* between clean-air days and highly polluted days is comparatively vague due to a smaller wind speed in the rural than the urban area. As shown in Fig. 12b, the diurnal variation of σ_w on highly polluted days is relatively inapparent, with a mean daily maximum value of 0.21 m s^{-1}. For TKE, e, a significant difference of mean diurnal variation under different pollution levels is shown in Fig. 12c. The mean daily maximum e on clean-air days is 0.79 m s^{-2}, but is only 0.33 m s^{-2} on highly polluted days. This characteristic is in agreement with Liu et al. (2011).

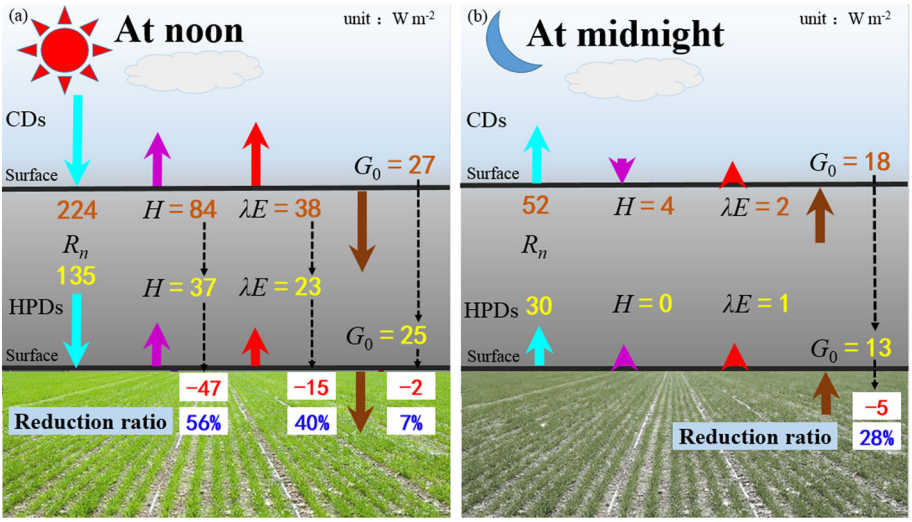

Fig. 10 Sketch map of surface energy budget. **a** The surface energy budget at 1200 LT, and **b** at 2400 LT. Units of W m^{-2}

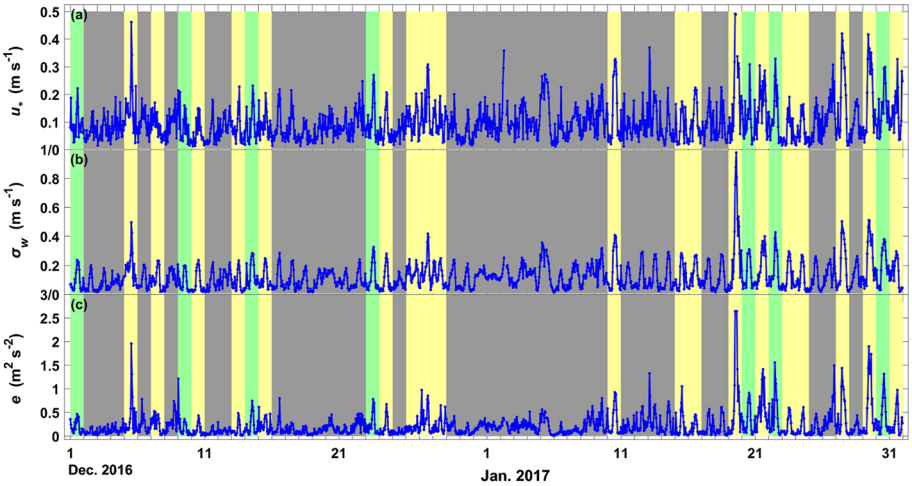

Fig. 11 Variations of measured, **a** u_*, **b** σ_w, and **c** e from December 1, 2016 through January 31, 2017 at the Gucheng measurement site. The green blocks, yellow blocks, and grey blocks represent clean air days, moderately polluted days, and highly polluted days, respectively

4 Discussion

We have examined the surface energy budget during a fog–haze event using observations from a field experiment in the North China Plain. However, the sample size is limited, and therefore results have statistical limitations. On the other hand, an inherent imbalance in the dataset between the three categories may cause biases in comparing the mean diurnal variation of variables under different polluted conditions. In the North China Plain, the haze

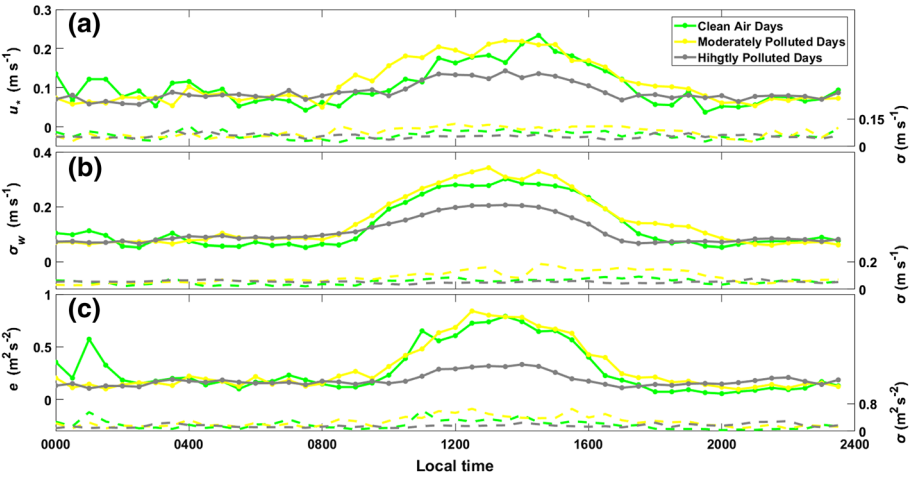

Fig. 12 The mean diurnal variation of **a** u_*, **b** σ_w, and **c** e under different conditions of pollution. The green line, yellow line, and grey line represent the mean value on clean-air days, moderately polluted days, and highly polluted days, respectively, dash lines are σ

events are concentrated in winter, especially in December and January, and obtain to more robust statistical results, long-term observations are required.

Although previous observational studies of the surface energy budget during haze events are rare, previous numerical simulation studies show results similar to our findings. For instance, based on Coupled Atmosphere-Plant-Soil model simulations. Yu et al. (2002) found that the aerosol-induced reduction of H (λE) was about 40 (20) W m^{-2} at noon for a wet-soil case, with a aerosol single-scattering albedo of 0.8. By using the WRF-Chem model, Gao et al. (2015) found that the aerosol-induced change in shortwave radiation flux, longwave radiation flux, H, and λE were around -105 W m^{-2}, 10 W m^{-2}, -46 W m^{-2}, and -16 W m^{-2} at noon in the Beijing-Hebei-Tianjin region from January 10 to January 15 2013.

In particular, clouds also have an influence on the radiation balance and surface energy budget. However, due to the lack of reliable cloud observation. we have not taken the impacts of clouds into account in our results. Satellite observations either mistake aerosols as clouds on highly polluted days [e.g., MODIS (Moderate-Resolution Image Spectroradiometer)] (Tan et al. 2017) or have a very low-time resolution [e.g., CALIPSO (Cloud-Aerosol Lidar and Infrared Pathfinder Satellite Observations)]. Effective methods to discriminate clouds from aerosols rely on ground-based measurements, such as sun photometers, total sky imagers, or micropulse lidars.

5 Conclusions

We have investigated the characteristics of meteorological conditions, the near-surface radiation balance, surface energy budget and turbulent parameters under different pollution conditions over a winter wheat field in the North China Plain by using observations made at the Gucheng station from December 1, 2016 through January 31, 2017. We conclude the following:

(1) Meteorological conditions with a lower wind speed, higher relative humidity, and lower surface pressure correspond to a higher $PM_{2.5}$ concentration. The correlation coefficients between daily mean $PM_{2.5}$ concentration and daily maximum (mean) wind speed, daily mean relative humidity, and daily mean surface pressure are -0.35 (-0.23), 0.47, and -0.56, respectively. Additionally, atmospheric stratification also closely relates to pollution process. Our results show a weaker unstable stratification during the daytime and a weaker stable stratification at night on highly polluted days.

(2) For $S_{\downarrow}$, we found that the range of diurnal variation was significantly smaller on highly polluted days than on clean-air days, the mean daily maximum $S_{\downarrow}$ is only 232 W m^{-2} on highly polluted days, however, the mean daily maximum $S_{\downarrow}$ reaches 387 W m^{-2} on clean-air days. The correlation coefficient between daily mean $PM_{2.5}$ concentration and daily mean $S_{\downarrow}$ is -0.54. The $L_{\downarrow}$ values are larger on highly polluted days than on clean-air days and the difference in mean $L_{\downarrow}$ between highly polluted days and clean-air days is 43 W m^{-2}. The correlation coefficient between daily mean $PM_{2.5}$ concentration and daily mean $L_{\downarrow}$ is 0.49. The values of R_n under different pollution levels also show striking differences. At night-time, R_n is controlled by $L_{\downarrow}$ and $L_{\uparrow}$, and compared to clean-air days, highly polluted days have an obviously larger $L_{\downarrow}$ and a similar $L_{\uparrow}$, which results in a larger R_n at night. The correlation coefficient between daily mean $PM_{2.5}$ concentration and night-time mean R_n is 0.51. On the other hand, during daytime, the influence of $S_{\downarrow}$ on R_n is significant, and the smaller daily maximum $S_{\downarrow}$ produces a smaller daily maximum R_n on highly polluted days. The mean daily maximum R_n on highly polluted days is less than 135 W m^{-2}.

(3) During the whole observation period, the range of diurnal variation of H and λE was diminished on highly polluted days; the mean daily maximum H (λE) was 40 (28) W m^{-2} on highly polluted days, but the mean daily maximum H (λE) on clean-air days was 90 (42) W m^{-2}. The correlation coefficient between daily mean $PM_{2.5}$ concentration and daily mean H (λE) was -0.36 (-0.32). During the night-time, H and λE were both close to zero under all pollution conditions. The mean daily maximum value of G_0 also decreased with the intensification of pollution.

(4) Compared to previous studies, a weaker distinction of u_* under different pollution levels was found in our research, which was caused by the low wind speed during the whole observation period. For e (σ_w), the mean daily maximum value on highly polluted days was only 0.33 m s^{-2} (0.21 m s^{-1}), but this value reached 0.79 m s^{-2} (0.30 m s^{-1}) on clean air days.

Overall, based on the observations from the field experiment, the feedbacks between a fog–haze event and physical processes in the boundary layer are quantitatively described herein, which provides a basis for setting up and/or evaluating climate model parameters. To further understand the generation mechanism and impacts of severe fog–haze pollution, analysis of the atmospheric background circulation, description of the vertical structure of the boundary layer, and tracking of the pollution sources are probably necessary.

Acknowledgements This study was supported by the National Key Research and Development Program of Ministry of Science and Technology of China (2016YFC0203304), and National Natural Science Foundation of China (41875013, 41275022, and 41711530223). We are grateful to the anonymous reviewers for their careful review and valuable comments, which led to substantial improvements in this manuscript.

References

Chan C, Yao X (2008) Air pollution in mega cities in China. Atmos Environ 42:1–42

Che H, Xia X, Zhu J, Li Z, Dubovik O, Holben B, Goloub P, Chen H, Estelles V, Cuevas-Agulló E, Blarel L, Wang H, Zhao H, Zhang X, Wang Y, Sun J, Tao R, Zhang X, Shi G (2014) Column aerosol optical properties and aerosol radiative forcing during a serious haze–fog month over North China Plain in 2013 based on ground-based sunphotometer measurements. Atmos Chem Phys 14:2125–2138

Chen H, Wang H (2015) Haze days in North China and the associated atmospheric circulations based on daily visibility data from 1960 to 2012. J Geophys Res Atmos 120:5895–5909

Ding Y, Liu Y (2014) Analysis of long-term variations of fog and haze in China in recent 50 years and their relations with atmospheric humidity. Sci China Earth Sci 57:36–46

Dupont JC, Haeffelin M, Badosa J, Elias T, Favez O, Petit JE, Meleux F, Sciare J, Crenn V, Bonne JL (2016) Role of the boundary layer dynamics effects on an extreme air pollution event in Paris. Atmos Environ 141:571–579

Foken T, Buck AL, Nye RA, Horn RD (1998) A Lyman-alpha hygrometer with variable path length. J Atmos Ocean Technol 15:211–214

Foken T, Leuning R, Oncley SR, Mauder M, Aubinet M (2012) Corrections and data quality control. In: Aubinet M, Vesala T, Papale D (eds) Eddy covariance: a practical guide to measurement and data analysis. Springer, New York, pp 85–131

Fu G, Xu W, Yang R, Li J, Zhao C (2014) The distribution and trends of fog and haze in the North China Plain over the past 30 years. Atmos Chem Phys 14:16123–16149

Gao Z, Chen GT, Hu Y (2007) Impact of soil vertical water movement on the energy balance of different land surface. Int J Biometeorol 51:565–573

Gao Z, Horton R, Liu HP (2010) Impact of wave phase different between soil surface heat flux and soil surface temperature on soil surface energy balance closure. J Geophys Res 115:D16112

Gao Y, Zhang M, Liu Z, Wang P, Xia X, Tao M, Zhu L (2015) Modeling the feedback between aerosol and meteorological variables in the atmospheric boundary layer during a severe fog–haze event over the North China Plain. Atmos Chem Phys 15:1093–1130

Garratt JR (1992) The atmospheric boundary layer. Cambridge University Press, Cambridge, UK

Guo X, Sun Y, Miao S (2016) Characterizing urban turbulence under haze pollution: insights into temperature–humidity dissimilarity. Boundary-Layer Meteorol 158:501–510

Li Z, Xia X, Cribb M, Mi W, Holben B, Wang P, Chen H, Tsay SC, Eck TF, Zhao F, Dutton EG, Dickerson RR (2007) Aerosol optical properties and their radiative effects in northern China. J Geophys Res Atmos 112:321–341

Lin W, Xu X, Ge B, Zhang X (2009) Characteristics of gaseous pollutants at Gucheng, a rural site southwest of Beijing. J Geophys Res 114:D00G14

Liu D, Yang J, Niu S, Li Z (2011) On the evolution and structure of a radiation fog event in Nanjing. J Adv Atmos Sci 28:223–237

Moncrieff J, Clement R, Finnigan J, Meyers T (2004) Averaging, detrending, and filtering of eddy covariance time series. In: Lee X, Massman W, Law B (eds) Handbook of micrometeorology: a guide for surface flux measurement and analysis. Kluwer Academic Publishers, Dordrecht, pp 7–31

Pahlow M, Kleissl J, Parlange MB (2005) Atmospheric boundary-layer structure observed during a haze event due to forest-fire smoke. Boundary-Layer Meteorol 114:53–70

Quan J, Zhang Q, He H, Liu J, Huang M, Jin H (2011) Analysis of the formation of fog and haze in North China Plain (NCP). Atmos Chem Phys 11:11911–11937

Ramanathan V, Crutzen PJ, Lelieveld J, Mitra AP, Althausen D, Anderson J, Andreae MO, Cantrell W, Cass GR, Chung CE, Clarke AD, Coakley JA, Collins WD, Conant WC, Dulac F, Heintzenberg J, Heymsfield AJ, Holben B, Howell S, Hudson J, Jayaraman A, Kiehl JT, Krishnamurti TN, Lubin D, McFarquhar G, Novakov T, Ogren JA, Podgorny IA, Prather K, Priestley K, Prospero JM, Quinn PK, Rajeev K, Rasch P, Rupert S, Sadourny R, Satheesh SK, Shaw GE, Sheridan P, Valero FPJ (2001) Indian ocean experiment: an integrated analysis of the climate forcing and effects of the great Indo-Asian haze. J Geophys Res Atmos 106:28371–28398

Tan SC, Zhang X, Wang H, Chen B, Shi GY, Shi C (2017) Comparisons of cloud detection among four satellite sensors on severe haze days in eastern china. Atmos Ocean Sci Lett 11:86–93

Wang, Y., Li, Z., Zhang, Y., Wang, Q., Ma, J.: Impact of aerosols on radiation during a heavy haze event in Beijing. In: IOP Conference Series: Earth Environmental Science—35th International Symposium on Remote Sensing of Environment, Beijing, China, vol. 17, p. 012012 (2014)

Wang Y, Che H, Ma J, Wang Q, Shi G, Chen H, Goloub P, Hao X (2009) Correction to "Aerosol radiative forcing under clear, hazy, foggy, and dusty weather conditions over Beijing, China". Geophys Res Lett 36:150–164

Wang S, Liao T, Wang L, Sun Y (2016) Process analysis of characteristics of the boundary layer during a heavy haze pollution episode in an inland megacity, China. J Environ Sci 40:138–144
Webb EK, Pearman GI, Leuning R (1980) Correction of flux measurements for density effects due to heat and water vapour transfer. Q J R Meteorol Soc 106:85–100
Xu WY, Zhao CS, Ran L, Deng ZZ, Liu PF, Ma N, Lin WL, Xu XB, Yan P, He X, Yu J, Liang WD, Chen LL (2011) Characteristics of pollutants and their correlation to meteorological conditions at a suburban site in the North China Plain. Atmos Chem Phys 11:4353–4369
Ye X, Song Y, Cai X, Zhang H (2015) Study on the synoptic flow patterns and boundary layer process of the severe haze events over the North China Plain in January 2013. Atmos Environ 124:129–145
Yu H, Liu S, Dickinson RE (2002) Radiative effects of aerosols on the evolution of the atmospheric boundary layer. J Geophys Res Atmos 107:3–14
Zhang R, Li Q, Zhang R (2014) Meteorological conditions for the persistent severe fog and haze event over eastern China in January 2013. Sci China Earth Sci 57:26–35
Zhao XJ, Zhao PS, Xu J, Meng W, Pu WW, Dong F, He D, Shi QF (2013) Analysis of a winter regional haze event and its formation mechanism in the North China Plain. Atmos Chem Phys 13:5685–5696

Affiliations

Changwei Liu[1] · Zhiqiu Gao[2,3] · Yubin Li[3] · Chloe Y. Gao[4] · Zhongbo Su[5] · Xiaoye Zhang[6]

✉ Zhiqiu Gao
zgao@mail.iap.ac.cn

1 Key Laboratory of Meteorological Disaster of Ministry of Education, Collaborative Innovation Centre on Forecast and Evaluation of Meteorological Disasters, School of Remote Sensing and Geomatics Engineering, Nanjing University of Information Science and Technology, Nanjing 210044, China

2 State Key Laboratory of Atmospheric Boundary Layer Physics and Atmospheric Chemistry, Institute of Atmospheric Physics, Chinese Academy of Sciences, Beijing 100029, China

3 Key Laboratory of Meteorological Disaster of Ministry of Education, Collaborative Innovation Centre on Forecast and Evaluation of Meteorological Disasters, School of Atmospheric Physics, Nanjing University of Information Science and Technology, Nanjing 210044, China

4 Department of Earth and Environmental Sciences, Columbia University, New York, NY 10027, USA

5 Faculty of Geo-Information Science and Earth Observation (ITC), University of Twente, Enschede, The Netherlands

6 Chinese Academy of Meteorological Sciences, Beijing 100081, China